Surface Diffusion Dynamics of a Single Polymer Chain in Dilute Solution

Hu-Jun Qian, Li-Jun Chen, Zhong-Yuan Lu,* and Ze-Sheng Li

State Key Laboratory of Theoretical and Computational Chemistry, Institute of Theoretical Chemistry, Jilin University, Changchun 130023, China

(Received 29 March 2007; published 6 August 2007)

Comprehensive three-dimensional dissipative particle dynamics simulations are carried out to elucidate the diffusion mechanism of a strongly adsorbed polymer chain on a solid surface in dilute solutions. We find Rouse and reptation dynamics for polymer chain diffusing on smooth and rough surfaces (with obstacles or sticking points), respectively. Combining with scaling analysis, we find that the interactions between the surface and the fluid screen the hydrodynamic interaction. The different scaling as found for a polymer chain diffusing on a fluid membrane [Phys. Rev. Lett. **82**, 1911 (1999)] and on a solid surface [Nature (London) **406**, 146 (2000)] may be explained by the solid surface inhomogeneity that induces reptation.

DOI: 10.1103/PhysRevLett.99.068301 PACS numbers: 82.35.Gh, 83.10.Rs, 83.80.Rs

Polymer diffusion dynamics is always fundamental. There is a good understanding of polymer diffusion in the bulk [1,2]. Recently, the diffusion dynamics of a strongly adsorbed chain on surfaces in dilute solution has come into focus [3–7], where the chain conformation assumes a ''pancake'' conformation in which its height normal to the surface is on the order of a monomer size and independent of the chain length N. The chain diffusion coefficient D was observed to scale with N as described by Rouse scaling, $D \sim N^{-1}$, for DNA diffusing on a fluid lipid membrane [3,4]. A stronger dependence of D on N which is actually reptationlike was found for polymer diffusing on solid surface, i.e., $D \sim N^{-3/2}$ [5,6].

In a work trying to explain the reasons for these contrasting scalings, Granick and co-workers had proposed several scenarios [6]. An implicit conjecture was first raised that hydrodynamic interactions (HI) might take effect in the case of a solid surface is not important in the case of membrane surface. Kumar, Granick and coworkers had endeavored to clarify the effect of HI on polymer surface diffusion with the aid of computer simulations [8,9]. In recent three-dimensional (3D) simulations with explicit solvent [9], the HI effect on chain diffusing on solid surfaces was still unclear. Specifically, they found different scalings for three *solid* surface models [9]. For the analytical smooth surface, $D \sim N^{-3/4}$ was found; for the smooth surface with no-slip boundary conditions and the corrugated surface, $D \sim N^{-1}$ was found. Their 3D simulation results reproduce the Rouse scaling of chain diffusing on fluid membrane [3,4], but do not reproduce the stronger $D \sim N^{-3/2}$ scaling found in experiments with solid surfaces [5,6].

The work described here is motivated to clarify the implicit conjecture about the importance of HI on polymer diffusing on solid surfaces and to explain the reasons for finding different dynamic scalings on different types of surfaces. Our simulations are carried out in 3D with explicit solvent, using the dissipative particle dynamics (DPD) simulation technique which can describe hydrodynamic phenomena in fluids properly. Inspiringly, we find Rouse scaling, $D \sim N^{-1}$, for a chain diffusing on smooth surfaces, and reptationlike scaling, $D \sim N^{-3/2}$, for a chain diffusing on inhomogeneous surfaces. Combining this with scaling analysis, we clarify that HI should be *absent* for finding reptation scaling on solid surfaces and this scaling is mainly due to the surface inhomogeneities including obstacles and sticking points. The results here are partially in harmony with those of Refs. [8,9].

Within the DPD method, all the particles interact with each other through three types of pairwise forces [10]: (i) a conservative force, F_{ij}^C; (ii) a dissipative force, F_{ij}^D; and (iii) a random force, F_{ij}^R. They take the forms of: $\mathbf{F}_{ij}^C = \alpha_{ij}\omega^C(r_{ij})\mathbf{e}_{ij}$, $\mathbf{F}_{ij}^D = -\gamma\omega^D(r_{ij})(\mathbf{v}_{ij}\cdot\mathbf{e}_{ij})\mathbf{e}_{ij}$, and $\mathbf{F}_{ij}^R = \sigma\omega^R(r_{ij})\xi_{ij}\Delta t^{-1/2}\mathbf{e}_{ij}$, where $\mathbf{r}_{ij} = \mathbf{r}_i - \mathbf{r}_j$, $r_{ij} = |\mathbf{r}_{ij}|$, $\mathbf{e}_{ij} = \mathbf{r}_{ij}/r_{ij}$, and $\mathbf{v}_{ij} = \mathbf{v}_i - \mathbf{v}_j$. ξ_{ij} are symmetric random numbers with zero mean and unit variance, and are chosen independently for each interacting pair of particles at each time step Δt. α_{ij} is a maximum repulsion between interacting particles i and j, and γ and σ are amplitudes of dissipative and random forces. $\omega^C(r_{ij})$, $\omega^D(r_{ij})$, and $\omega^R(r_{ij})$ are weight functions for the corresponding forces, respectively. The dissipative forces are proportional to the relative velocities of the interacting pairs, which represent the friction between particles and account for energy loss, while the random forces compensate for lost degrees of freedom due to coarse graining and act as a heat source to heat up the system. According to the fluctuation dissipation theorem, the dissipative and random forces are coupled together to ensure the thermodynamic equilibrium [11] by the relations of $\omega^D(r) = [\omega^R(r)]^2 = (1-r)^2$, and $\sigma^2 = 2\gamma k_B T$. The forces act over all particles within a cutoff radius $r_c = 1$, beyond which the forces are considered negligible. The pairwise nature of the dissipative and random forces ensures local momentum conservation leading to correct long-range hydrodynamics [12]. The polymer

chain is constructed by a bead-spring model with the spring force $\mathbf{F}_{ij}^{s} = -k\mathbf{r}_{ij}$ ($k = 10$) in our simulations.

For a solid-liquid interface, we expect density distortions at microscopic length scale (MLS), but the distortions will disappear as we increase the length scale. Thus we adopt two different techniques to impose accurately the no-slip wall boundary condition with [13] and without [14] density distortions to mimic solid surfaces at small and large length scales (LLS), respectively. The surface is modeled by 2 layers of freezing DPD particles distributed on a regular lattice. Below we give brief descriptions of the two algorithms; more details about these two techniques can be found in Refs. [13,14], respectively.

At MLS, the effective interaction parameter α_{wf} between the wall and the fluid particles are adjusted according to the fact that the average force per unit area F_w exerted by the wall within one cutoff radius should be equal to the total force per unit area from the fluid, F_f. F_f is parameterized as the product of a constant 0.39 and the pressure of the system [13]. We obtain a second-order polynomial fit for total wall force in the range of density values from 3 to 25, $F_w = \alpha_{wf}(0.023\,86\rho_w^2 + 0.656\,83\rho_w - 1.166\,09)$. This fitting curve deviates slightly from that shown in Ref. [13] at large wall densities. If we calculate this total force with 4 layers of frozen particles in the wall region, we obtain the same fitting curve as shown in Fig. 9 of Ref. [13]. This may be ascribed to the fact that the interaction between the frozen wall image and the fluid particles is not neglected in Ref. [13]. However, at low particle density in the wall ($\rho_w = 3$, which is adopted in this research), the total force possesses the same value for the wall model with 2 and 4 layers. Therefore, we choose $\alpha_w = (3.2447 \times 25.0)^{1/2} \simeq 9.0$ as in Ref. [13].

At LLS, a self-consistent algorithm which is called adaptive boundary conditions [14] is adopted to update the fluid-surface interaction force based on the density deviation from the desired distribution near to the solid surface. The normal component of the force $\mathbf{F}_w^z(i_b)$ exerted by wall in the predivided bins near to the surface are adjusted according to $\mathbf{F}_w^z(i_b) = \mathbf{F}_w^z(i_b) + C_w[\sum_{i=i_a}^{i_b}\rho_s(i)/\sum_{i=i_a}^{i_b}\rho_d(i) - 1]$, where i_b is the bin index, C_w is a positive constant, $\rho_s(i)$ are the local density values averaged up to n_{av} bins [from i_a to i_b, $i_b = \max(i_b - n_{\mathrm{av}} + 1, 1)$], and $\rho_d(i)$ are desired density values in the same bins. In our simulations, the force adjusting range is one interaction cutoff radius. This computational domain is divided into $N_b = 5$ bins. The density value in bin i_b is obtained by a time average over $N_{\mathrm{av}} = 500$ time steps. The other parameters are $n_{\mathrm{av}} = 3$ and $C_w = 1$.

Test runs for Poiseuille flow with an external body force equal to 0.02 in a box with size of $10 \times 10 \times 10$ are carried out for these two surface models. The velocity, the temperature, and the density profiles are shown in Fig. 1(a) for MLS, and in (b) for LLS, respectively.

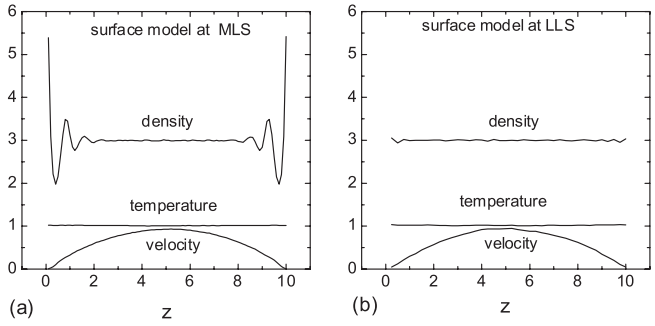

FIG. 1. Velocity, temperature, and density profiles for Poiseuille flow corresponding to two different boundary conditions at (a) MLS and (b) LLS.

The simulated surface models include: (a1) 2D surface randomly decorated by impenetrable obstacles with number density $c = 0.015625$ (In the following 3D rough surface models, we have adopted the same obstacle density); (b1) a smooth surface in 3D box with density distortions near to the surface (i.e., at MLS); (b2) a rough surface in 3D box with one-site obstacles distributed randomly at MLS; (c1) a smooth surface in 3D box without density distortions near to the surface (i.e., at LLS); (c2) a rough surface in 3D box with one-site obstacles regularly distributed at LLS; (c3) similar to (c2) but with large obstacles (nearest 9 surface particles are united together to form one obstacle); (c4) obstacles in (c2) are changed to sticking points by weakening the repulsions between these points and the polymer particles from $\alpha_{ij} = 200.0$ to -2.0. The interaction parameters α_{ij} between different types of particles in these models are

$$\alpha_{ij} = \begin{pmatrix} & p & s & w & o & st \\ p & 25.0 & 20.0 & 2.0 & 200.0 & -2.0 \\ s & 20.0 & 25.0 & 9.0 & 200.0 & 9.0 \\ w & 2.0 & 9.0 & 25.0 & 25.0 & 25.0 \\ o & 200.0 & 200.0 & 25.0 & 25.0 & / \\ st & -2.0 & 9.0 & 25.0 & / & 25.0 \end{pmatrix},$$

in which p, s, w, o, and st denote the particle for the polymer chain, the solvent, the solid wall, the obstacles, and the sticking points, respectively. We have carefully checked the parameter space and selected the parameters in a balance between keeping strong chain adsorption as a pancake and saving simulation time. The size of the simulation box is $40 \times 40 \times 8$, which is large enough in the lateral direction to avoid the interaction between the chain and its images.

To validate our DPD method, we first construct a 2D model (a1), which is analogous to that in Ref. [8]. Good agreement is found: i.e., $R_g \sim N^{3/4}$ and $D \sim N^{-3/2}$. The scaling relation between D and N is shown in Fig. 2(a1). This result in two dimensions cannot truly be used to explain the real experiments for chain diffusing on solid surface in the presence of explicit solvent [9]. Comprehensive simulations in three dimensions reported below

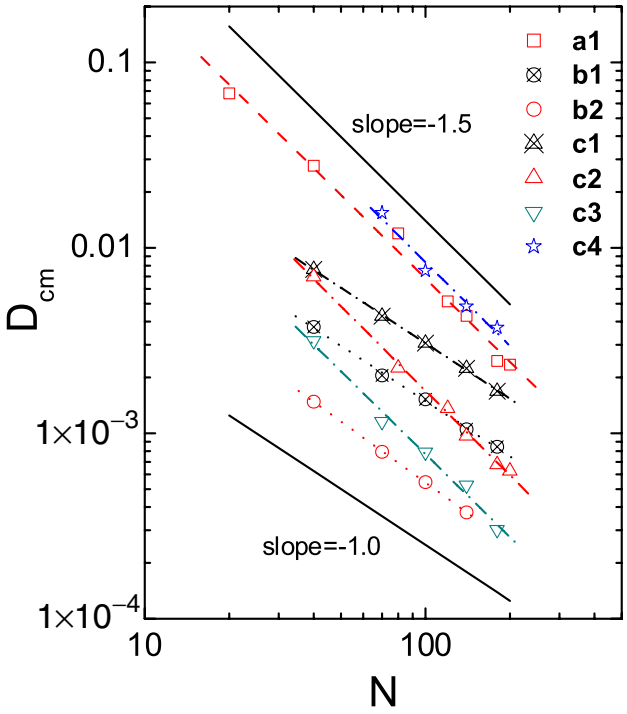

FIG. 2 (color online). The self-diffusion coefficient D of the center of mass of polymer chain, calculated via Einstein relation, is shown as a function of chain length N. Solid lines with slopes of -1.0 and -1.5 are drawn for comparison. The other lines represent the best fit of the data points to a power law about of -1.0 and -1.5, respectively. The symbols refer to the models: (a1) 2D model with regularly distributed obstacles; (b1) 3D smooth surface at MLS; (b2) 3D rough surface at MLS with obstacles randomly distributed; (c1) 3D smooth surface at LLS; (c2) 3D rough surface with regularly distributed obstacles at LLS; (c3) 3D rough surface with regularly distributed big obstacles at LLS; (c4) 3D surface with regularly distributed sticking points at LLS.

may compensate this weakness and be more valuable to describe the diffusion of polymer chain on surface in dilute solutions.

For a smooth surface at MLS [model (b1)], the wall particles interact with the fluid particles homogeneously. The scaling between D and N shows Rouse behavior [Fig. 2(b1)]. This is consistent with the result for the third surface model with no-slip boundary conditions in 3D molecular dynamics (MD) simulations [9]. It actually implies that HI is screened due to the interactions between fluid and surface particles. If HI were not screened, polymer dynamics should obey Zimm scaling in dilute solution, where the diffusion coefficient is reciprocally proportional to its size R, $D \sim k_B T/\zeta_Z \sim k_B T/\eta_s R \sim N^{-3/4}$ as shown for the first surface model in Ref. [9], in which $\zeta_Z \approx \eta_s R$ is the friction coefficient of the chain of size R being pulled through a solvent of viscosity η_s according to Stokes law. For a smooth surface at LLS [i.e., without density distortions near to the surface, model (c1)], we also obtain Rouse scaling [Fig. 2(c1)]. The absence of HI on the surface can also be rationalized as follows: suppose that the chain adsorbed on the surface takes the pancake conformation as discussed in Ref. [5], it will diffuse in a very thin layer near to the surface. The momentum is not conserved in this layer because of the reflection of particles at the surface, so HI does not exist in the region very near to the surface.

Granick *et al.* argued that including hydrodynamic interactions might rationalize the results in their experiments on a solid surface [6]. However, the emergence of Rouse behavior in our 3D simulations suggests that HI is also absent on solid surface. This result indeed further implies that, the difference between the dynamic scaling of adsorbed polymers on fluidic and solid surfaces may be from other influences, such as the solid surface inhomogeneity [8,15]. But for a rough surface with randomly distributed obstacles [model (b2)], we still find the Rouse scaling [Fig. 2(b2)]. This is because the polymer chain has the possibility to be trapped in the free spaces formed by the surrounding obstacles; it cannot reptate along its own primitive paths.

Because the randomness of the obstacle distribution makes the system much more complicated, we thus choose typical regular distributed obstacle models. For rough surfaces at LLS [models (c2) and (c3)], the obstacles are distributed regularly to avoid the trapping problem. For these models, we observe the reptation scaling behavior, $D \sim N^{-3/2}$ [Fig. 2(c2)(c3)]. The reptation scaling is also found for the surface with sticking points [Fig. 2(c4)].

We can directly visualize the Rouse and reptation behavior by plotting the primitive paths of the polymer chain, which with $N = 180$ in model (c1),(c2),(c3), and (c4) are taken as examples, as shown in Fig. 3. It is clear that on smooth surface (c1), the polymer chain is free to diffuse in any direction on the surface [(1) in Fig. 3]. But for rough surface (c2), the diffusion of polymer chain is confined between the obstacles [(2) in Fig. 3]. Such a confinement effect is more obvious for surface (c3) with big obstacles [(3) in Fig. 3]. On sticking surface (c4), polymer chain moves efficiently along its contour in a caterpillarlike fashion [(4) in Fig. 3] which is analogous to the reptation scenario supposed by Granick and co-workers [6].

Actually, the scaling relation of $D \sim N^{-3/2}$ on rough solid surfaces also implies that the HI is screened in these systems. The reptation model for the polymer melts is based on Gaussian chain statistics and the fact that the HI is screened by the entanglements in the melts, so the curvilinear diffusion coefficient D_c that describes motion of the chain along the tube simply obeys Rouse scaling, $D_c \sim N^{-1}$. Thus, the reptation time $\tau_{\text{rep}} \sim \langle L \rangle^2/D_c \sim N^3$, in which $\langle L \rangle \sim aN/N_e \sim bN(N_e)^{-1/2}$ is the average contour length of the primitive path, and N_e the number of monomers in a blob of size equal to the tube diameter $a \sim bN_e^{1/2}$. The reptation diffusion coefficient then follows Fick's law, $D_{\text{rep}} \sim R_g^2/\tau_{\text{rep}} \sim N^{-2}$, where $R_g \sim N^{1/2}$ is the radius of gyration of Gaussian chains. But in our simulations, the chain statistics is non-Gaussian with $R_g \sim N^{3/4}$ which is also obtained in experiments [3–7]. If we

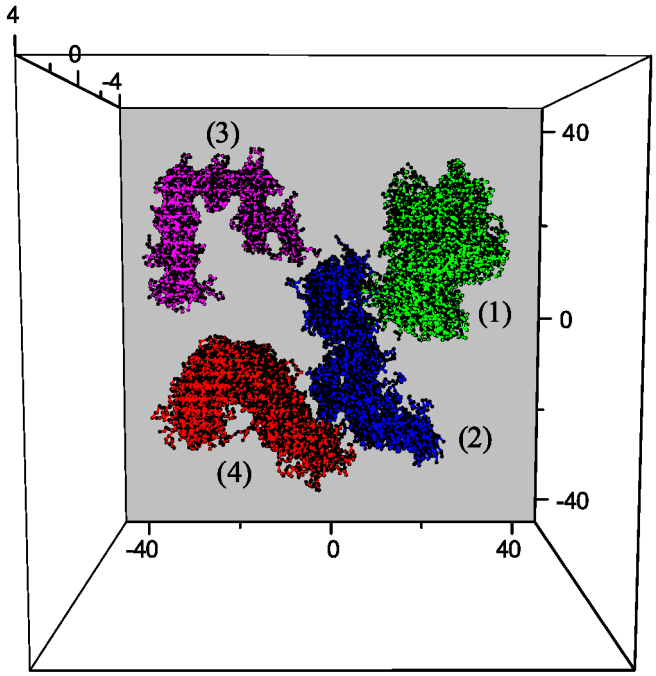

FIG. 3 (color online). Each snapshot represents the superposition of 40 configurations for a chain with length $N = 180$. The configurations are taken with 250 DPD time units apart; thus, the total time is 10 000. (1) Green: at smooth surface (c1), (2) blue: at rough surface (c2), (3) magenta: at rough surface (c3), and (4) red: at sticking surface (c4).

accept the reptation ansatz for the dilute solution in this study, and take into account the HI as argued by Granick *et al.* for solid surfaces, curvilinear diffusion coefficient D_c will be reciprocally proportional to chain size as discussed above according to Zimm model for dilute solutions, $D_c \sim k_B T/\zeta_Z \sim k_B T/\eta_s R \sim N^{-3/4}$. The reptational tube diameter $a \sim bN_e^{3/4}$ is approximately equal to the spacing length between obstacles, this results in the total length of the primitive path $\langle L\rangle \sim aN/N_e \sim bNN_e^{-1/4}$. Thus the reptation time is $\tau_{\text{rep}} \sim \langle L\rangle^2/D_c \sim N^{2.75}$, and $D_{\text{rep}} \sim R_g^2/\tau_{\text{rep}} \sim N^{-1.25}$ for reptation of chain on solid surface *with* HI. This conflicts with the experimental results and our simulations. Thus HI is actually screened for rough (and smooth) solid surface as for the membrane surface. The reptation scaling may come from the solid surface inhomogeneity with HI screened. In such a scenario of rough surface model, the polymer chain reptates between the obstacles or along the sticking points decorated on the surface, which correspond to surface inhomogeneities (chemical or physical) in the real experimental systems. The curvilinear diffusion coefficient is simply $D_c \sim N^{-1}$ according to Rouse model because there is no HI, the tube length is still $\langle L\rangle \sim bNN_e^{-1/4}$, and the reptation time $\tau_{\text{rep}} \sim \langle L\rangle^2/D_c \sim N^3$. This results in $D_{\text{rep}} \sim R_g^2/\tau_{\text{rep}} \sim N^{-1.5}$ for reptation of chain on solid surface *without* HI, which is found in experiments and our simulations.

In conclusion, we show a comprehensive 3D DPD simulation study to investigate the diffusion mechanism of strongly adsorbed polymer chain on solid surface in dilute solutions. A Rouse scaling $D \sim N^{-1}$ for chain diffusing on smooth solid surface, and a reptationlike scaling $D \sim N^{-3/2}$ for chain diffusing on inhomogeneous solid surfaces (with obstacles or sticking points), are obtained. Actually, similar results about crossover from Rouse to reptation regimes for diffusion dynamics of polymers confined on surfaces were obtained in wetting experiments [16]. Their results in essence evidence ours. Combing these simulation results with scaling analysis, we invalidate an implicit conjecture about the importance of HI on chain diffusing on solid surfaces in the literatures, and clarify that the *surface inhomogeneity* and the *absence of HI* is the reason for the appearance of different dynamic scalings in the cases of fluid membrane and the solid surfaces.

This work is supported by the National Science Foundation of China (No. 20490220 and No. 20404005), and JLSTP (No. 20050562).

*luzhy@mail.jlu.edu.cn

[1] M. Doi and S. F. Edwards, *Theory of Polymer Dynamics* (Clarendon, Oxford, 1986).
[2] M. Rubinstein and R. H. Colby, *Polymer Physics* (Oxford University, Oxford, 2003).
[3] B. Maier and J. O. Rädler, Phys. Rev. Lett. **82**, 1911 (1999).
[4] B. Maier and J. O. Rädler, Macromolecules **33**, 7185 (2000).
[5] S. A. Sukhishvili, Y. Chen, J. D. Müller, E. Grantton, K. S. Schweizer, and S. Granick, Nature (London) **406**, 146 (2000).
[6] S. A. Sukhishvili, Y. Chen, J. D. Müller, E. Grantton, K. S. Schweizer, and S. Granick, Macromolecules **35**, 1776 (2002).
[7] L. Zhang and S. Granick, Proc. Natl. Acad. Sci. U.S.A. **102**, 9118 (2005).
[8] T. G. Desai, P. Keblinski, S. K. Kumar, and S. Granick, J. Chem. Phys. **124**, 084904 (2006).
[9] T. G. Desai, P. Keblinski, S. K. Kumar, and S. Granick, Phys. Rev. Lett. **98**, 218301 (2007).
[10] R. D. Groot and P. B. Warren, J. Chem. Phys. **107**, 4423 (1997).
[11] P. Español and P. B. Warren, Europhys. Lett. **30**, 191 (1995).
[12] I. Pagonabarraga, M. H. J. Hagen, and D. Frenkel, Europhys. Lett. **42**, 377 (1998).
[13] I. V. Pivkin and G. E. Karniadakis, J. Comput. Phys. **207**, 114 (2005).
[14] I. V. Pivkin and G. E. Karniadakis, Phys. Rev. Lett. **96**, 206001 (2006).
[15] R. Azuma and H. Takayama, J. Chem. Phys. **111**, 8666 (1999).
[16] M. P. Valignat, G. Oshanin, S. Villette, A. M. Cazabat, and M. Moreau, Phys. Rev. Lett. **80**, 5377 (1998).